Discover Oncology

Research

Expression of CLDN1 and EGFR in PTC

JunJie Wu[1] · YouMei Wang[1] · Lei Yan[1] · YaWen Dong[1]

Received: 9 July 2024 / Accepted: 4 October 2024
Published online: 15 October 2024

Abstract
Papillary thyroid carcinoma (PTC) involves complex genetic mechanisms, notably involving CLDN1 and EGFR. This study investigates the expression and variations of these genes and their effects on tumor behavior and patient outcomes. Meta-analysis of CLDN1 and EGFR expression in TCGA–PTC patients and GEO datasets was conducted. cBioPortal was used for clinical analysis. GSEA, GO, KEGG, Hallmark pathways, and cibersort analysis were applied. Cell proliferation, migration, invasion, and apoptosis were assessed in vitro. Co-culturing with $CD8^+$ T cells, MTT assay, ELISA, subcutaneous tumor models, and immunohistochemistry were performed. TGF-β pathway-related proteins were analyzed via Western blot. CLDN1 and EGFR were overexpressed in PTC tumors, correlating with higher-risk patients and reduced $CD8^+$ T cell infiltration. Silencing these genes inhibited tumor cell functions and enhanced $CD8^+$ T cell activity, both in vitro and in vivo. CLDN1 and EGFR are crucial in PTC, linked to tumor invasiveness, EMT, and immune suppression, presenting them as potential therapeutic targets.

Keywords Papillary thyroid carcinoma · CLDN1 · EGFR · Epithelial–mesenchymal transition · Meta-analysis

1 Introduction

Papillary Thyroid Carcinoma (PTC) is an increasingly prevalent malignant tumor posing a significant challenge to global public health [1–3]. As the most common type of thyroid cancer, the treatment and management of PTC significantly impact patient quality of life and survival rates [3–5]. Despite most patients with PTC having a favorable long-term prognosis, the risk of post-surgical recurrence and resistance to traditional radiotherapy and chemotherapy remain critical concerns in treatment strategies [6]. These issues not only add to the psychological and economic burden of patients but also challenge the efficient allocation and utilization of medical resources. Therefore, exploring the pathophysiological mechanisms of PTC and identifying new therapeutic targets is essential for enhancing treatment outcomes and improving patients' quality of life.

The progression of PTC involves a complex interplay of numerous genes and molecular pathways [7]. Recent advances in molecular biology and genomics have gradually unveiled a series of gene mutations playing pivotal roles in the pathogenesis of PTC [2, 4, 8]. Mutations in the BRAF and RAS genes are among the most common molecular events in PTC development, affecting tumor cell proliferation, survival, invasiveness, metastatic capability, and treatment response [9, 10]. Furthermore, non-mutational molecular markers such as Claudin-1 (CLDN1) and Epidermal Growth Factor Receptor

Supplementary Information The online version contains supplementary material available at https://doi.org/10.1007/s12672-024-01428-9.

✉ YaWen Dong, 15824332645@163.com; JunJie Wu, wjjde987654321@163.com; YouMei Wang, 13511363960@163.com; Lei Yan, yanlei20240515@163.com | [1]Department of Pathology, the First People's Hospital of Pinghu, Jiaxing, Zhejiang, People's Republic of China.

(EGFR) have demonstrated significant roles in regulating PTC cell behavior. The expression and activity changes in these molecules are closely linked to tumor progression, invasiveness, and metastatic potential, offering new perspectives in understanding the pathophysiology of PTC [11].

Claudin-1 (CLDN1) is a tight junction protein primarily located on the cell membrane, playing a crucial role in forming tight junctions between cells and regulating paracellular permeability. In tumor cells, CLDN1 expression is often upregulated, which is closely associated with tumor invasion and metastasis. For example, in gastric cancer, increased CLDN1 expression promotes tumor cell proliferation and metastasis [12]. A study by Piontek et al. found that CLDN1 is highly expressed in PTC cells, supporting its potential as a molecular therapeutic target [13].

Epidermal Growth Factor Receptor (EGFR) is a transmembrane tyrosine kinase primarily located on the cell membrane, involved in regulating cell growth, division, and survival. Abnormal expression of EGFR is observed in various tumors, including non-small cell lung cancer, pancreatic cancer, and head and neck cancers, making it a significant therapeutic target in oncology [14]. However, despite extensive research on the roles of CLDN1 and EGFR in various tumors, their mechanisms of action within the PTC-specific environment and interactions with the tumor microenvironment, immune escape, and epithelial-mesenchymal transition (EMT) processes remain incompletely understood [15, 16]. Existing studies indicate that these molecules play crucial roles in promoting tumor cell proliferation, invasion, and migration, potentially correlating with disease severity and patient prognosis [17–19]. However, much of this research focuses on cancers other than PTC, with a limited understanding of the specific roles and expression differences of CLDN1 and EGFR in PTC, particularly regarding their impacts on tumor behavior and patient prognosis across different pathological subtypes.

Moreover, current studies have not adequately assessed the expression patterns, genetic variations of CLDN1 and EGFR in PTC, and their correlation with tumor progression, immune escape, and EMT processes [15, 16]. The lack of comprehensive analysis of these molecular markers restricts a full understanding of PTC's complex pathology and hinders further exploration of these molecules as potential therapeutic targets. Thus, systematically evaluating the roles of these molecules in PTC not only enhances our knowledge of the disease's molecular mechanisms but also may provide crucial insights for developing new therapeutic strategies.

In light of this background, this study aims to deeply investigate the expression patterns and genetic variations of CLDN1 and EGFR in PTC, along with their associations with tumor progression, immune escape, and EMT processes, by employing an integrated approach of transcriptome sequencing, meta-analysis, and public database resources. Through these analyses, we hope to reveal the mechanisms by which these molecules contribute to PTC development and assess their potential as biomarkers and therapeutic targets.

2 Materials and methods

2.1 Data acquisition and preparation

The clinical and transcriptomic data for PTC used in this study were sourced from The Cancer Genome Atlas (TCGA) database. All thyroid cancer patients' transcriptomic and clinical data were downloaded via the UCSC Xena platform. Clinical pathology information filtering yielded a total of 353 PTC patients, including both clinical information and gene expression data. Additionally, PTC-related transcriptomic RNA sequencing datasets were downloaded from the Gene Expression Omnibus (GEO) database (https://www.ncbi.nlm.nih.gov/geo/) for meta-analysis, as detailed in Table S1. Since these data were obtained from public databases, obtaining ethical committee approval was not required.

2.2 GSEA analysis

In this study, Gene Set Enrichment Analysis (GSEA) was conducted using the Signal-to-Noise ratio (Signal2Noise) method for ranking metrics, with all other parameters set to their default values. GSEA was performed using the OmicShare tool. This analysis incorporated the Gene Ontology (GO) and the Kyoto Encyclopedia of Genes and Genomes (KEGG), as well as the Hallmark gene sets, to provide a comprehensive overview of the biological signals. The analyses were conducted on the Omicshare platform [20].

2.3 cBioPortal online analysis

To investigate the expression differences of CLDN1 and EGFR across various cancer samples, data analysis was carried out using the cBioPortal database (https://www.cbioportal.org/). The TCGA PTC cohort was selected to retrieve gene expression data. After data acquisition, CLDN1 and EGFR gene expression data were categorized into median groups using the built-in analysis tools of cBioPortal, and the clinical characteristics of the high and low expression groups were examined through the website [21].

2.4 HPA database analysis

To investigate the differential expression of CLDN1 and EGFR proteins across various tumor types and their corresponding normal tissues, the Human Protein Atlas (HPA) database (https://www.proteinatlas.org/) was utilized. Extensive immunohistochemical analysis data on the expression patterns of human proteins in diverse tissues and cells were provided by the HPA database. For CLDN1 and EGFR proteins, the database was searched for immunohistochemistry (IHC) results in a variety of tumor tissues and corresponding normal tissues [22].

2.5 Gene set download and correlation analysis

To explore the correlation between CLDN1 and EGFR and the genes involved in the EMT pathway, gene sets were downloaded from MsigDB with the pathway name "REACTOME_TGF_BETA_SIGNALING_IN_EMT_EPITHELIAL_TO_MESENCHYMAL_TRANSITION," comprising 16 genes. The correlation plots for the two genes were generated using the R package ggstatsplot (v0.11.1), and the multi-gene correlation plots were visualized with the R package pheatmap (v1.0.12). Spearman's rank correlation analysis was employed to assess the relationship between non-normally distributed quantitative variables, considering p-values less than 0.05 as statistically significant [23] (Figure S1).

2.6 Meta-analysis

Meta-analysis was conducted using the meta for the package (version 4.4.0) in R, with the effect size estimated as the mean difference (MD) alongside its 95% confidence interval (CI). The aim of heterogeneity testing (i.e., testing for consistency across studies) was to determine the feasibility of pooling the individual studies, utilizing the Q test and chi-squared test. Heterogeneity was assessed based on the I^2 value and P-value. The absence of statistical heterogeneity, indicated by a P-value greater than 0.05 and an I^2 value less than 50%, suggests that the variations across studies are attributable to sampling error, permitting the use of a fixed-effect model for the meta-analysis. Conversely, significant statistical heterogeneity, reflected by a P-value less than 0.05 and an I^2 value exceeding 50%, necessitates the adoption of a random-effects model for pooling the results [24].

2.7 Cell culture

The normal thyroid epithelial cell line (HT-ori3)—CBP61205 and three PTC cell lines (IHH-4, SNU-790, TPC-1)—with catalog numbers CBP61201, CBP61209, and CBP60257, respectively, were purchased from Nanjing KeyGen Biotech. These cells were cultured in RPMI-1640 medium from Gibco (USA) supplemented with 10% fetal bovine serum (10099158), 100 U/mL penicillin, and 100 mg/L streptomycin (15140148). The cells were maintained at 37 °C in a 5% CO_2 environment with the medium changed every 2 days. Passaging was performed when cell confluence reached 80% to 90%, and cells in logarithmic growth phase were used for experiments. Human $CD8^+$ T cells were obtained from Huizhi Yuan Biological Technology (Suzhou) Co., Ltd. (082A04.11) and cultured in high-glucose RPMI-1640 medium (R8758, Sigma-Aldrich, USA) containing 4.5 g/L glucose for experimentation [25].

2.8 Cell processing and grouping

TPC-1 cells in logarithmic growth phase were digested with trypsin, centrifuged, and resuspended at a concentration of 5×10^4 cells/mL. The cells were then seeded into 6-well plates at a volume of 2 mL per well. Prior to constructing the in vitro cell model, lentiviruses (MOI = 10, viral titer of 1×10^8 TU/mL) were added to the cell culture medium. Post 48 h, stable cell lines were selected using 2 μg/mL puromycin (UC0E03, Sigma-Aldrich, USA) for a duration of 2 weeks. The

cell transfection groups were as follows: (1) sh-NC group: transfected with sh-NC lentivirus; (2) sh-CLDN1-1 group: transfected with sh-CLDN1-1 lentivirus; (3) sh-CLDN1-2 group: transfected with sh-CLDN1-2 lentivirus; (4) sh-EGFR-1 group: transfected with sh-EGFR-1 lentivirus; (5) sh-EGFR-2 group: transfected with sh-EGFR-2 lentivirus. The lentiviral vectors used were designed and synthesized by Guangzhou Ruibo Biotechnology Co., Ltd [26].

For the co-culture and grouping: (1) sh-NC group: TPC-1 cells transfected with sh-NC lentivirus were co-cultured with $CD8^+$ T cells; (2) sh-CLDN1 group: TPC-1 cells transfected with sh-CLDN1 lentivirus were co-cultured with $CD8^+$ T cells; (3) sh-EGFR group: TPC-1 cells transfected with sh-EGFR lentivirus were co-cultured with $CD8^+$ T cells. TPC-1 cells and $CD8^+$ T cells were co-cultured in a shared system at 37 °C, 5% CO_2 for 48 h. TPC-1 cells were placed in the upper chamber, while $CD8^+$ T cells were seeded in the lower chamber of a Transwell plate (CLS3412, Corning, USA). Separated by a 0.4 μm membrane, soluble factors were allowed to pass through, while the cells were kept separate. After 3 days, the supernatant and cultured cells were collected for further experiments [27].

2.9 Flow cytometry

Cell apoptosis rate was determined using the Annexin V-FITC Cell Apoptosis Detection Kit (C1062S, Beyotime, Shanghai). Cell density was adjusted to 1×10^5 cells/mL, and 3 mL of cell suspension was centrifuged twice at 500 rpm for 5 min each time in a 10 mL centrifuge tube. After removing the culture medium, cells were resuspended in 100 μL binding buffer, and 5 μL each of Annexin V-FITC and PI were added. The mixture was gently vortexed, kept in the dark at room temperature for 15 min, and then analyzed using flow cytometry to detect FITC and PI fluorescence. Quadrants were defined as follows: Q1: upper left quadrant (UL) representing cell debris without intact membranes or cells undergoing death for other reasons; Q2: upper right quadrant (UR) indicating late apoptotic cells; Q3: lower left quadrant (LL) representing normal (viable) cells; Q4: lower right quadrant (LR) indicating early apoptotic cells. Statistical analysis focused on quadrants Q2 and Q4 to determine the apoptosis rate [28].

2.10 Enzyme-linked immunosorbent assay (ELISA)

IFN-γ (ab174443, Abcam) and Granzyme B (ab235635, Abcam) levels in the extracellular model were measured using ELISA kits according to the manufacturer's instructions [29].

2.11 EDU experiment for assessing cell proliferation

The cells of interest were seeded in a 24-well plate and EdU (C10310-2, Guangzhou RiboBio Co., Ltd., Guangzhou) was added to the culture medium to achieve a concentration of 10 μmol/L. The cells were then incubated in a cell culture incubator for 2 h. After removing the culture medium, the cells were fixed with a PBS solution containing 4% paraformaldehyde at room temperature for 15 min. The cells were then washed twice with PBS containing 3% BSA, incubated at room temperature with PBS containing 0.5% Triton-100 for 20 min, followed by two washes with PBS containing 3% BSA. Subsequently, 100 μL of staining solution was added to each well and incubated at room temperature in the dark for 30 min. DAPI nuclear staining was performed for 5 min, and after sealing the slides, 6–10 random fields were observed under a fluorescence microscope (BX63, Olympus, Japan). The number of positive cells in each field was recorded. The EdU labeling rate (%) was calculated as the number of positive cells divided by the sum of positive and negative cells, multiplied by 100% [30].

2.12 Wound healing assay for cell migration

Using a marker pen, uniform horizontal lines were drawn on the back of a 6-well plate, spaced 1 cm apart, crossing over the wells. Approximately 5×10^5 cells were seeded in each well, cultured until confluence reached 100%, and then a straight scratch was made across the cell layer at the marked line using a pipette tip perpendicular to the cell surface. After scratching, the plate was washed three times with sterile PBS to remove non-adherent cells, ensuring the gap created by scratching was clearly visible. Fresh serum-free culture medium was added, and the cells were incubated at 37 °C in a 5% CO_2 incubator. After 24 h, the width of the scratch was observed under a microscope, photographed, and the results were recorded. The migration rate analysis was performed using Image J software [31].

2.13 Transwell experiment for assessing cell invasion capability

ECM gel (E1270, Sigma-Aldrich, Germany) was added to the upper chamber of a 24-well Transwell plate (8 μm) and incubated in a 37 °C incubator for 30 min to allow the gel to solidify. Cells transfected for 48 h were collected, resuspended in serum-free culture medium at a concentration of 10^5 cells, and seeded in the upper chamber with 200 μL of cell suspension (2×10^4 cells/well) in the Transwell plate. The lower chamber was filled with 800 μL of culture medium containing 20% FBS. After incubating for 24 h at 37 °C, the Transwell plate was removed, washed twice with PBS, fixed with formaldehyde for 10 min, and then rinsed thrice with water. The cells were stained with 0.1% crystal violet, left at room temperature for 30 min, washed twice with PBS, and the cells on the upper surface were wiped off with a cotton ball. The invaded cells were photographed using an inverted optical microscope (CKX53, Olympus, Japan), and their invasion capability was quantified and analyzed using Image J software [32].

2.14 MTT assay for measuring cell viability

The cells of interest were seeded in a 96-well cell culture plate at a density of $3–5 \times 10^4$ cells/mL and cultured for 48 h. MTT solution (10 mg/mL, ST316, Beyotime Biotechnology Co., Ltd, Shanghai) was added to the cell suspension and incubated for 4 h, followed by the addition of DMSO with shaking for 10 min. The absorbance (OD 490 nm) was measured using a spectrophotometer (Laspec, China) to assess cell viability [33].

2.15 qRT-PCR

Total RNA was extracted from tissues or cells using Trizol reagent (15596026, Invitrogen, USA), and the concentration and purity of total RNA were assessed at 260/280 nm using NanoDrop LITE (ND-LITE-PR, Thermo Scientific™, USA). The extracted total RNA was reverse transcribed into cDNA using the PrimeScript RT reagent Kit with gDNA Eraser (RR047Q, TaKaRa, Japan). Subsequently, the expression levels of each gene were measured by RT-qPCR using SYBR Green PCR Master Mix reagents (4364344, Applied Biosystems, USA) and the ABI PRISM 7500 Sequence Detection System (Applied Biosystems).

The primers for each gene were synthesized by TaKaRa (Table S2), with GAPDH serving as the reference gene. The relative expression levels of each gene were analyzed using the $2^{-\Delta\Delta Ct}$ method, where ΔΔCt = (average Ct value of the target gene in the experimental group – average Ct value of the reference gene in the experimental group) – (average Ct value of the target gene in the control group – average Ct value of the reference gene in the control group) [34].

2.16 Western blot analysis

Tissues or cells were collected and lysed with enhanced RIPA lysis buffer (containing a proteinase inhibitor) from Beyotime Biotechnology Co., Ltd, Shanghai (Product code: P0013B) to extract total proteins. The protein concentration of each sample was determined using a BCA protein quantification kit (Product code: P0012, Beyotime Biotechnology Co., Ltd, Shanghai), and 30 μg of protein was loaded per lane after adjusting with deionized water. A 12.5% SDS separating gel and a stacking gel were prepared. The samples were mixed with loading buffer, boiled at 100 °C for 5 min, cooled on ice, centrifuged, and equal amounts were loaded onto each lane for electrophoresis separation. The proteins were then transferred from the gel onto a PVDF membrane. The membrane was blocked with 5% skim milk powder at 4 °C overnight, followed by incubation with primary antibodies: rabbit anti-CLDN1 (1:800, ab307692, Abcam, Cambridge, UK), EGFR (1:200–2000, ab52894, Abcam, Cambridge, UK), TGFβ1 (1:1000, ab215715, Abcam, Cambridge, UK), TGFβR1 (1:1000, ab235578, Abcam, Cambridge, UK), TGFβR2 (1:1000, ab283230, Abcam, Cambridge, UK), and GAPDH (1:1000, ab9485, Abcam, Cambridge, UK), overnight at 4 °C. The membrane was washed thrice with PBS at room temperature for 5 min each, followed by incubation with goat anti-rabbit IgG HRP-conjugated secondary antibody (1:5000, ab6721, Abcam, Cambridge, UK) for 1 h at 37 °C. After washing the membrane thrice with PBS buffer at room temperature for 5 min each, an equal amount of Pierce™ ECL Western Blotting Substrate (32209, Thermo Scientific™, USA) components A and B were mixed in a darkroom, added to the membrane, and exposed in

a gel imaging system. The bands in the Western blot images were quantified for grayscale using the Bio-Rad imaging system (BIO-RAD, USA) and ImageJ analysis software, with GAPDH as the internal control [35].

2.17 Establishment of subcutaneous tumor model in mice

Thirty-six male NOD-SCID mice aged 4–6 weeks and weighing 15–25 g were purchased from Beijing Vital River Laboratory Animal Technology Co., Ltd (Beijing, China). The NOD-SCID mice were housed in an SPF-level animal laboratory and acclimatized for 1 week to observe their status. The animal experimental processes were approved by the Ethnic Committee of Pinghu First People's Hospital (CMUXN2023083) and conducted in strict accordance to the standard of the Guide for the Care and Use of Laboratory Animals published by the Ministry of Science and Technology of the People's Republic of China in 2006.

Stable TPC-1 cells with knocked down CLDN1 and EGFR (sh-CLDN1, sh-EGFR) or TPC-1 cells transfected with control lentivirus (sh-NC cells) were injected subcutaneously into the flank of the mice in a volume of 100 µL PBS containing 5×10^6 cells. The mice were divided into three groups, each comprising 6 mice: sh-NC group (injected with sh-NC cells), sh-CLDN1 group (injected with sh-CLDN1 cells), and sh-EGFR group (injected with sh-EGFR cells). On the 5th day post-injection, each mouse was intravenously administered 200 µL of PBS-suspended 1×10^7 $CD8^+$ T cells [36]. Thirty days post-injection, the mice were euthanized. Tumor diameters were measured using a caliper, and tumor volume was calculated using the formula: (longest diameter × shortest diameter^2 × 0.5). Tumor tissues from the mice were collected, embedded in paraffin, and subjected to immunohistochemical analysis to evaluate the expression of CD8 and Granzyme B proteins. The animal experiments were approved by our institutional review board [37].

2.18 Immunohistochemistry

After embedding and sectioning the tumor tissues from each group of mice, the slides were baked at 60 °C for 20 min. Subsequently, the slides were sequentially immersed in xylene solution for 15 min, followed by immersion in absolute alcohol for 5 min, and then changed to fresh absolute alcohol for an additional 5 min. The slides were then hydrated by sequential immersion in 95% and 70% ethanol for 10 min each. A 3% H_2O_2 solution was added to each slide and allowed to react at room temperature for 10 min to block endogenous peroxidases. Citrate buffer was added, and the slides were microwaved for 3 min. Antigen retrieval solution was applied, and the slides were left at room temperature for 10 min, followed by washing with PBS three times. Normal goat serum blocking solution (E510009, Shanghai Sangon Biotech) was added and incubated at room temperature for 20 min.

Primary antibodies CD8 (MA1-7632, Thermo Fisher, 1:200) and Granzyme B (14-8822-82, Thermo Fisher, 1:200, RRID: AB_468530) were added dropwise. The slides were then incubated overnight at 4 °C, washed with PBS three times, and incubated with goat anti-rabbit IgG secondary antibody (ab6721, 1:500, Abcam, UK) for 30 min. After washing with PBS, the slides were subjected to DAB chromogenic reagent (Sigma, USA), where drops of color developers A, B, and C were added to the specimen and left for 6 min for color development. Post-coloring, the specimens were briefly stained with hematoxylin for 30 s, followed by dehydration in increasing grades of ethanol (70%, 80%, 90%, 95%), and then immersed twice in absolute ethanol for 5 min each. Finally, the specimens were sealed using neutral resin. The sections were observed under a light microscope (BX63, Olympus, Japan). The proportion of positive cells expressing the protein was measured using an image analysis system (Aperio Scanscope System, Vista, CA). For assessing the proportion of follicular tissue, the area of follicular tissue within the field of view was calculated, with the ratio determined as follicular tissue area/total tissue area. Ten random samples were taken for analysis [38, 39].

2.19 Statistical methods

In this study, the statistical analysis was conducted using GraphPad Prism software version 8.0. Descriptive statistics were reported as mean ± standard deviation for continuous variables. The comparison between the two groups was performed using an independent samples t-test. For comparisons among multiple groups, a one-way analysis of variance (ANOVA) was employed. Statistical significance was considered at a threshold of $P < 0.05$.

3 Results and discussion

3.1 Expression patterns and clinical relevance of CLDN1 and EGFR in PTC

In our investigation of PTC, we observed a significant correlation between the expressions of CLDN1 and EGFR (Fig. 1A), suggesting a possible synergistic role in thyroid cancer development. By analyzing PTC expression data from TCGA, we found that both CLDN1 and EGFR expressions were significantly upregulated in tumor tissues compared to normal tissues ($P < 0.05$) (Fig. 1B, C). Further validation through meta-analysis of multiple PTC-related transcriptomic RNA sequencing datasets from the GEO database, combined with TCGA–PTC data, indicated significant overexpression of CLDN1 (MD = 2.58, 95% CI = 1.07–4.09) and EGFR (MD = 0.34, 95% CI = 0.02–0.66) in PTC tumor tissues compared to normal controls (Figs. 1D, E). Subsequent analysis based on the HPA database revealed higher protein expression levels of CLDN1 and EGFR in tumor tissues of PTC patients (Fig. 1F–I). These findings indicate that mRNA and protein expressions of CLDN1 and EGFR are significantly elevated in PTC tumor tissues compared to normal tissues, underscoring their potential as biomarkers and therapeutic targets in PTC management.

3.2 Association between CLDN1 and EGFR expression and clinical characteristics of PTC

In this study, a detailed analysis of the expression levels of CLDN1 and EGFR in PTC patients revealed significant associations with several clinical features, showing similar patterns of influence. Notably, high-expression groups exhibited a higher prevalence of Braf-like characteristics and a lower incidence of Ras-like features compared to the low-expression groups in the context of BRAF600E and RAS mutations (Fig. 2A, B). Furthermore, patients within the high-expression cohorts for both CLDN1 and EGFR had a greater proportion of high-risk classifications (Fig. 2C, D), suggesting the involvement of these gene expressions in disease progression and severity.

3.3 Gene function enrichment and immune infiltration correlation of CLDN1 and EGFR in PTC

This study conducted a single-sample GSEA on CLDN1 and EGFR gene expressions in PTC, dividing patients into low and high-expression groups to analyze differential gene enrichment. The analysis identified significant enrichment in five key pathways, including EMT, TNFα signaling via NFκB, TGFβ signaling, protein secretion, and mitotic spindle assembly (Fig. 3A). GO pathway analysis revealed significant associations with processes such as the establishment and maintenance of cell polarity, Hippo signaling pathway, protein secretion, and K48-linked ubiquitination (Fig. 3B). In KEGG pathway analysis, significant enrichment was observed in processes related to extracellular matrix-receptor interaction, cytoskeletal regulation, apoptosis, TGFβ signaling, and cell junction organization (Fig. 3C). These results suggest a close association of CLDN1 and EGFR with the EMT mechanism and several signaling pathways, potentially influencing PTC development and prognosis.

Furthermore, this study employed the CIBERSORT algorithm for quantitative analysis of immune cell infiltration in PTC patients, comparing the differences between high and low CLDN1 and EGFR expression groups. CIBERSORT facilitated the estimation of the relative abundance of various immune cells within the tumor microenvironment. The analysis indicated that the high gene set score groups had increased proportions of naive B cells, $CD4^+$ resident memory T cells, and activated dendritic cells, with decreased frequencies of memory B cells, plasma cells, $CD8^+$ T cells, and M1 macrophages (Fig. 3D). Notably, groups with high expression of CLDN1 and EGFR exhibited lower proportions of $CD8^+$ T cells, suggesting that CLDN1 and EGFR might suppress antitumor immunity by affecting $CD8^+$ T cell presence. These findings reveal that CLDN1 and EGFR may play roles in modulating immune cell infiltration in the PTC microenvironment.

3.4 Correlation between CLDN1, EGFR, and the EMT pathway in PTC

In our analysis of the gene pathway scores within the PTC cohort, we discovered a probable link between CLDN1 and EGFR and the EMT pathway, suggesting their roles in the EMT process of thyroid cancer. Notably, invasive PTC frequently exhibits characteristics of EMT [40]. Further correlation analysis revealed a significant positive relationship between CLDN1 and EGFR genes and the EMT pathway ($R^2 = 0.34$, $p = 2.72e{-}12$; $R^2 = 0.15$, $p = 2.09e{-}03$) (Fig. 4A, B). Particularly, within the analysis of the TGFB receptor-mediated EMT gene set, both CLDN1 and EGFR showed significant positive

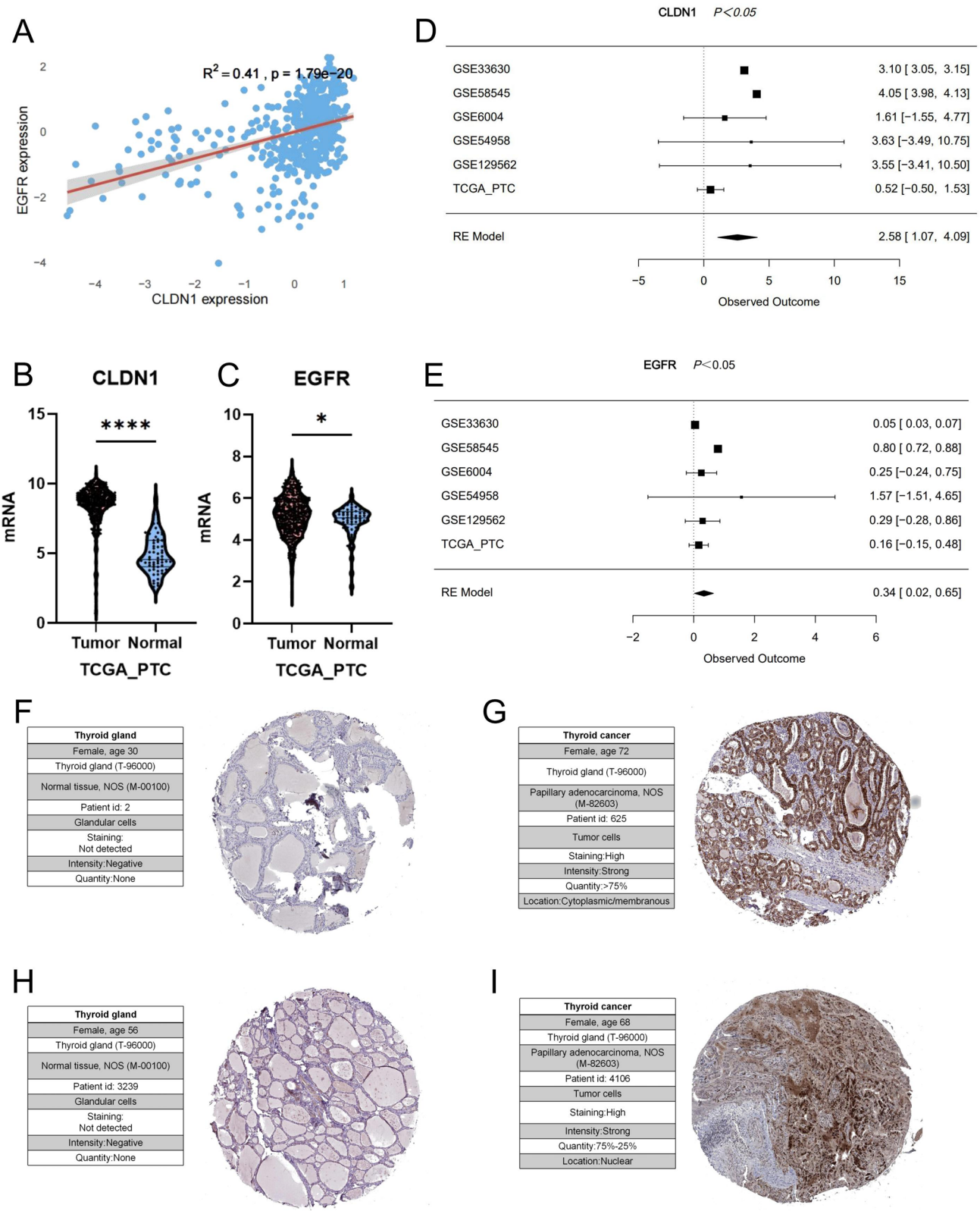

Fig. 1 Correlation and meta-analysis of CLDN1 and EGFR expression in PTC. **A** Scatter plot showing the correlation between CLDN1 and EGFR expression in the TCGA PTC dataset; **B** violin plot of CLDN1 expression in tumor vs. normal tissues in the TCGA–PTC dataset; **C** violin plot of EGFR expression in tumor vs. normal tissues in the TCGA–PTC dataset; **D** forest plot of the meta-analysis on differential expression of CLDN1 in PTC; **E** forest plot of the meta-analysis on differential expression of EGFR in PTC; **F** representative image of CLDN1 expression in normal thyroid tissue; **G** representative image of CLDN1 expression in PTC tissue; **H** representative image of EGFR expression in normal thyroid tissue; **I** representative image of EGFR expression in PTC tissue

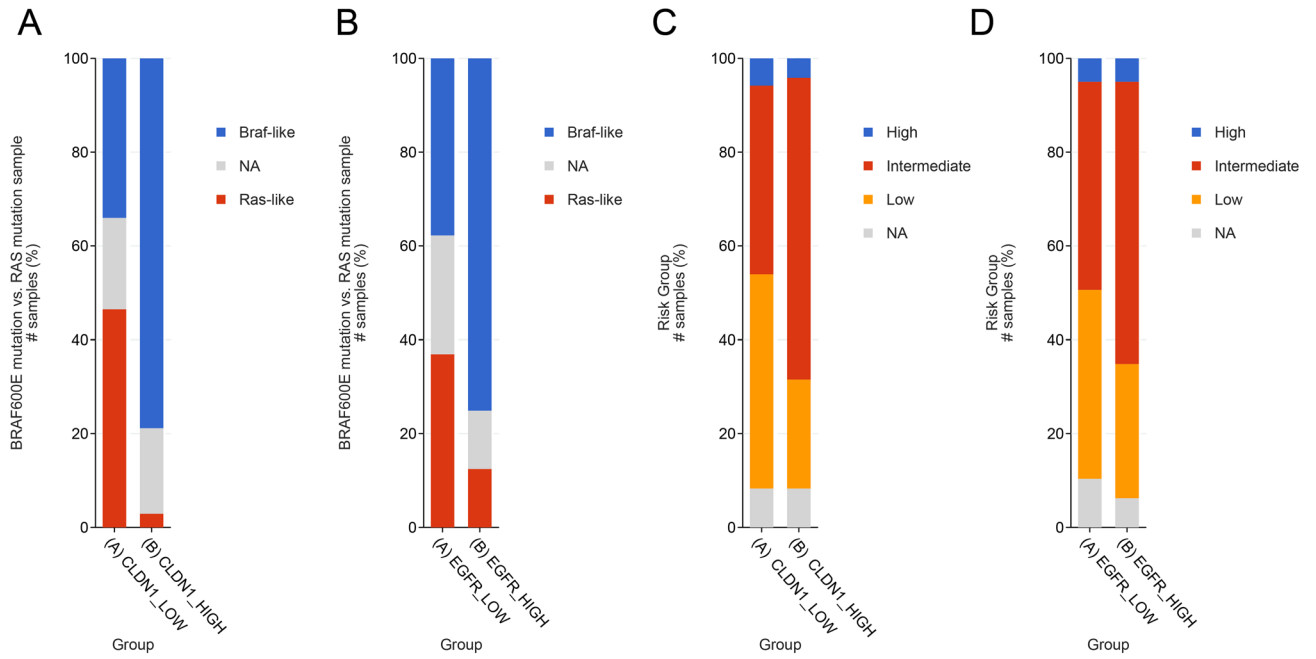

Fig. 2 Association between CLDN1 and EGFR expression levels and clinical information distribution in PTC. **A** Bar graph showing the distribution of BRAF600E and RAS mutations between high and low median expression groups of CLDN1; **B** bar graph showing the distribution of BRAF600E and RAS mutations between high and low median expression groups of EGFR; **C** bar graph showing risk levels between high and low median expression groups of CLDN1; **D** bar graph showing risk levels between high and low median expression groups of EGFR

correlations with several genes, including TGFB1, TGFBR1, and TGFBR2 (Fig. 4C). These genes are crucial components of the TGF-β receptor signaling pathway during the EMT process, further reinforcing the connection between CLDN1 and EGFR and EMT-related pathways in PTC.

3.5 Effects of CLDN1 and EGFR on the biological activity of PTC cells

The bioinformatics results indicate that the expression levels of CLDN1 and EGFR may impact the EMT pathway, thereby influencing tumor behavior. To validate these findings, we selected one normal thyroid epithelial cell line (HT-ori3) and three PTC cell lines (IHH-4, SNU-790, TPC-1). The expression levels of CLDN1 and EGFR mRNA and protein in each cell were examined using qRT-PCR and WB. Results revealed a significant increase in CLDN1 and EGFR mRNA and protein levels in the PTC cell lines (IHH-4, SNU-790, TPC-1) compared to the normal thyroid epithelial cell line (HT-ori3), with TPC-1 showing the highest expression, thus chosen for subsequent experiments (Fig. 5A, B).

To investigate the impact of CLDN1 and EGFR on the biological activity of PTC cells, TPC-1 cells were subjected to CLDN1 and EGFR silencing treatments. qRT-PCR results demonstrated (Fig. 5C) a significant reduction in CLDN1 expression in the sh-CLDN1-1 and sh-CLDN1-2 groups compared to the sh-NC group, with sh-CLDN1-1 showing better efficacy and selected for subsequent experiments. Similarly, a significant decrease in EGFR expression was observed in the sh-EGFR-1 and sh-EGFR-2 groups compared to the sh-NC group, with sh-EGFR-2 showing better efficacy and being chosen for subsequent experiments.

Proliferation ability of PTC cells was assessed using EDU, migration and invasion capabilities were examined through scratch and Transwell assays, and apoptosis rate was measured by flow cytometry. Results indicated that compared to the sh-NC group, the sh-CLDN1 and sh-EGFR groups exhibited significantly suppressed the proliferation, migration, and invasion abilities of PTC cells, along with a notable increase in apoptosis rate (Fig. 5D–G).

WB analysis of TGF-β receptor signaling pathway factors TGFβ1, TGFβR1, and TGFβR2 proteins during the EMT process in PTC cells revealed a significant decrease in the expression of these proteins in the sh-CLDN1 and sh-EGFR groups compared to the sh-NC group (Fig. 5H).

These findings suggest that silencing CLDN1 and EGFR can inhibit proliferation, migration, and invasion capabilities of TPC-1 cells and promote cell apoptosis in PTC.

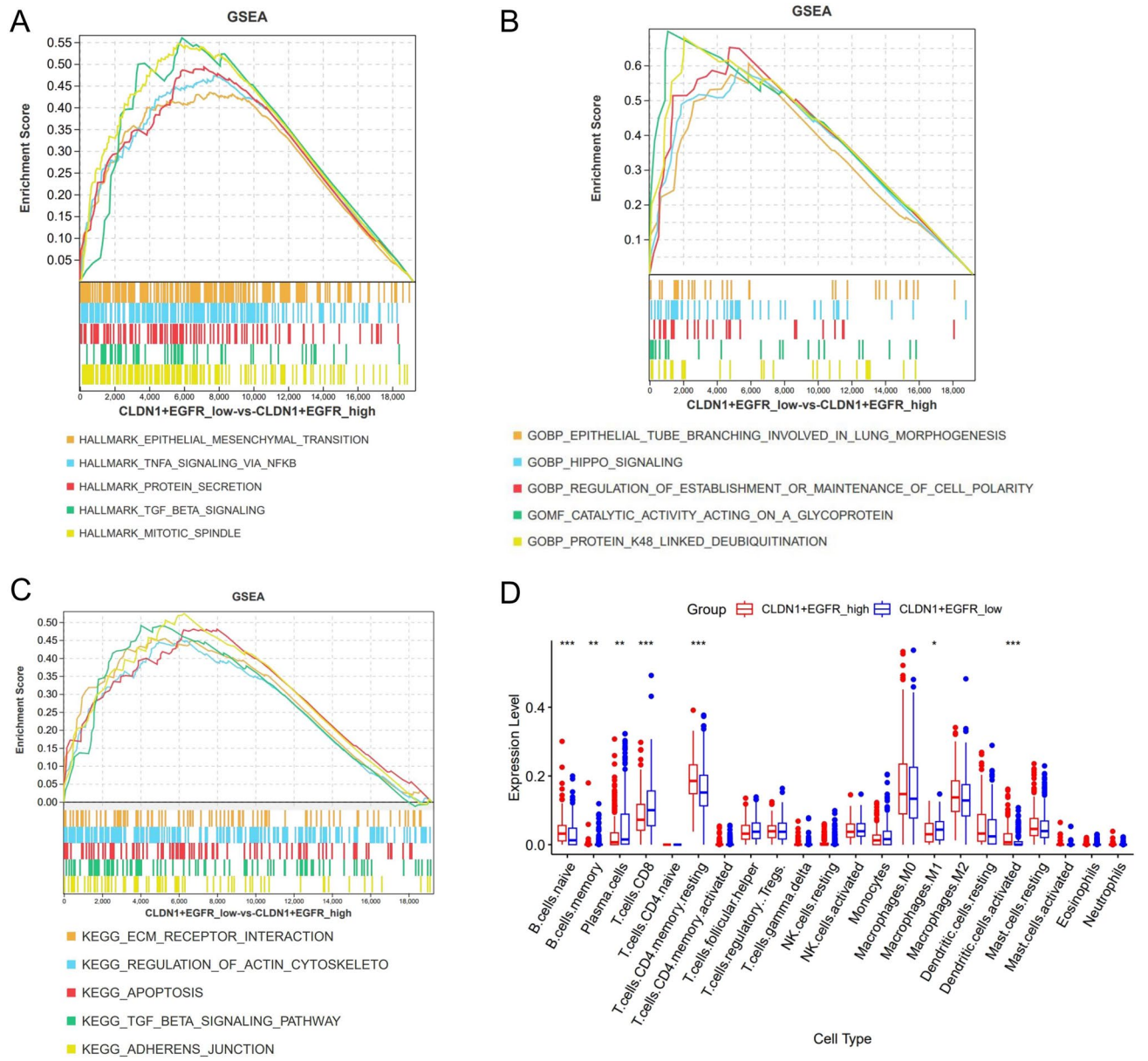

Fig. 3 Functional enrichment and immune infiltration correlation analysis of differential gene expression in PTC based on CLDN1 and EGFR. **A** GSEA analysis of HALLMARK pathways based on CLDN1 and EGFR gene expression groups; **B** GSEA analysis of GO pathways based on CLDN1 and EGFR gene expression groups; **C** GSEA analysis of KEGG pathways based on CLDN1 and EGFR gene expression groups; **D** boxplot of immune cell infiltration based on CLDN1 and EGFR gene expression groups

3.6 Silencing CLDN1 and EGFR in PTC cells affects the activity and cytotoxicity of co-cultured CD8$^+$ T cells

The bioinformatics results suggest that the groups with high expression of CLDN1 and EGFR have a lower proportion of CD8$^+$ T cells, indicating that CLDN1 and EGFR may inhibit anti-tumor immunity by affecting CD8$^+$ T cells. To further elucidate the impact of CLDN1 and EGFR expression levels in PTC cells on CD8$^+$ T cells, TPC-1 cells with knocked-down CLDN1 and EGFR were co-cultured with activated CD8$^+$ T cells for 48 h. The MTT assay was employed to assess CD8$^+$ T cell viability, revealing a significant increase in the viability of CD8$^+$ T cells co-cultured with sh-CLDN1 and sh-EGFR groups compared to the sh-NC group (Fig. 6A).

Existing literature has confirmed that granule enzyme B (GZMB) and interferon-gamma (IFN-γ) secreted by CD8$^+$ T cells can enhance their ability to identify and kill tumor cells [41]. ELISA experiments were conducted to measure

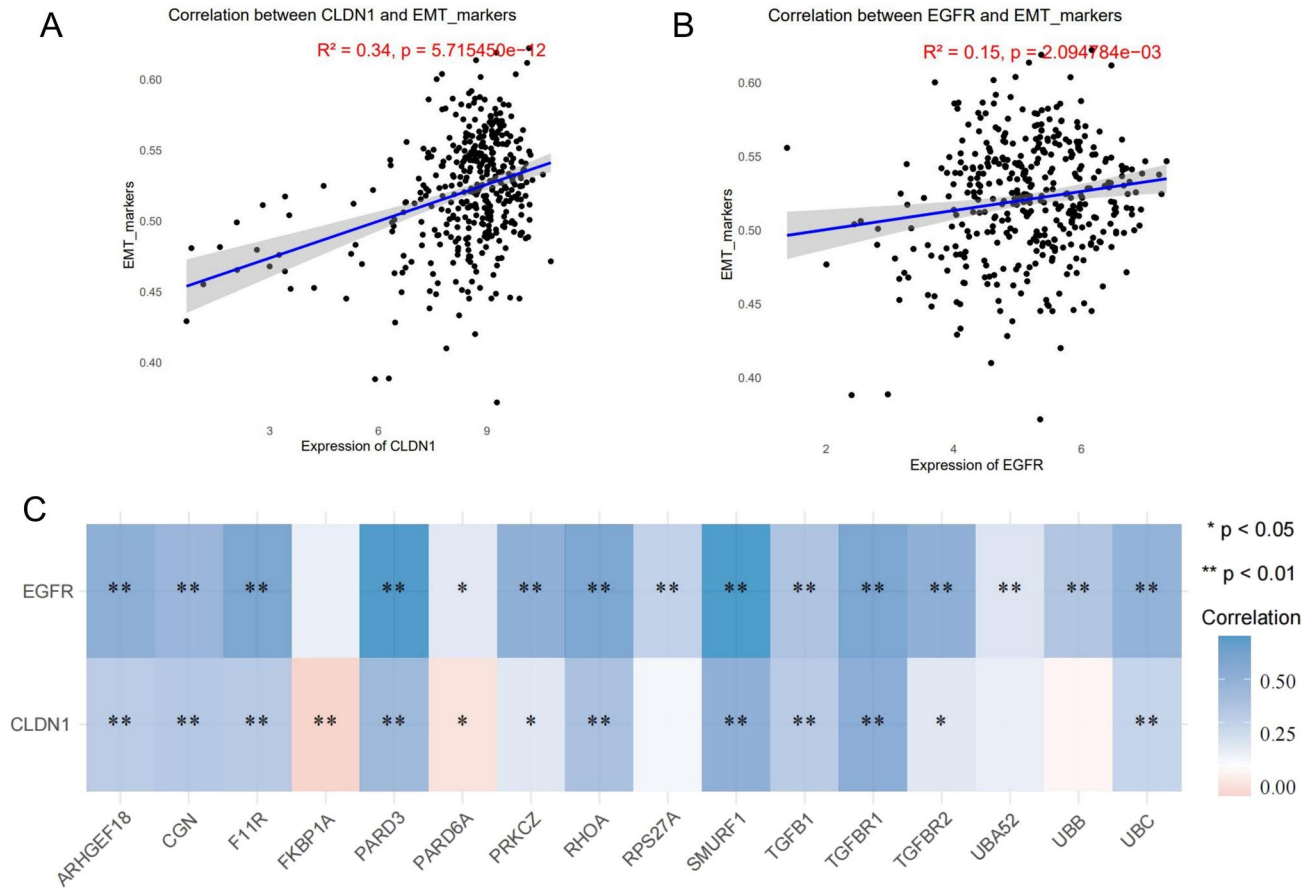

Fig. 4 Correlation analysis of CLDN1 and EGFR gene expression with the EMT pathway in PTC. **A** Scatter plot of CLDN1 gene expression correlation with EMT marker genes in TCGA–PTC; **B** scatter plot of EGFR gene expression correlation with EMT marker genes in TCGA–PTC; **C** heatmap showing the correlation of CLDN1, EGFR with EMT genes

the secretion of GZMB and IFN-γ cell factors in the supernatant of different cell groups. The results showed a significant increase in GZMB and IFN-γ in the supernatant of $CD8^+$ T cells co-cultured with sh-CLDN1 and sh-EGFR groups compared to the sh-NC group (Fig. 6B, C).

These results demonstrate that silencing CLDN1 and EGFR in PTC cells can enhance the activity and cytotoxicity of co-cultured $CD8^+$ T cells.

3.7 The impact of CLDN1 and EGFR silencing on tumor formation ability of thyroid papillary carcinoma cells in vivo and upregulation of $CD8^+$ T cell immune function

In vitro cell experiments have confirmed that silencing CLDN1 and EGFR in thyroid papillary carcinoma cells can inhibit the biological activity of thyroid cancer and enhance the co-culture activity and cytotoxicity of $CD8^+$ T cells. To validate whether this mechanism affects the tumor-forming ability of cancer cells in mice, thyroid papillary carcinoma cells with stable knockdown of CLDN1 and EGFR were injected subcutaneously into mice. Tumor volume changes were measured every 5 days, and mice were euthanized after 30 days to measure tumor weight. The results showed that compared to the sh-NC group, the sh-CLDN1 and sh-EGFR groups exhibited significantly reduced tumor volume and weight (Fig. 7A–C).

Western blot analysis was conducted on tumor tissues from each group to examine the expression of proteins related to the TGF-β receptor signaling pathway during the EMT process, including TGFB1, TGFBR1, and TGFBR2. The results indicated a significant decrease in the expression of TGFB1, TGFBR1, and TGFBR2 proteins in the tumor tissues of mice in the sh-CLDN1 and sh-EGFR groups compared to the sh-NC group (Fig. 7D).

Furthermore, to investigate the impact of CLDN1 and EGFR on tumor immune cells, immunohistochemical staining was performed. It was observed that compared to the sh-NC group, the infiltration of $CD8^+$ cells and granzyme B^+ cells in tumor tissue slices was significantly increased in the sh-CLDN1 and sh-EGFR groups (Fig. 7E).

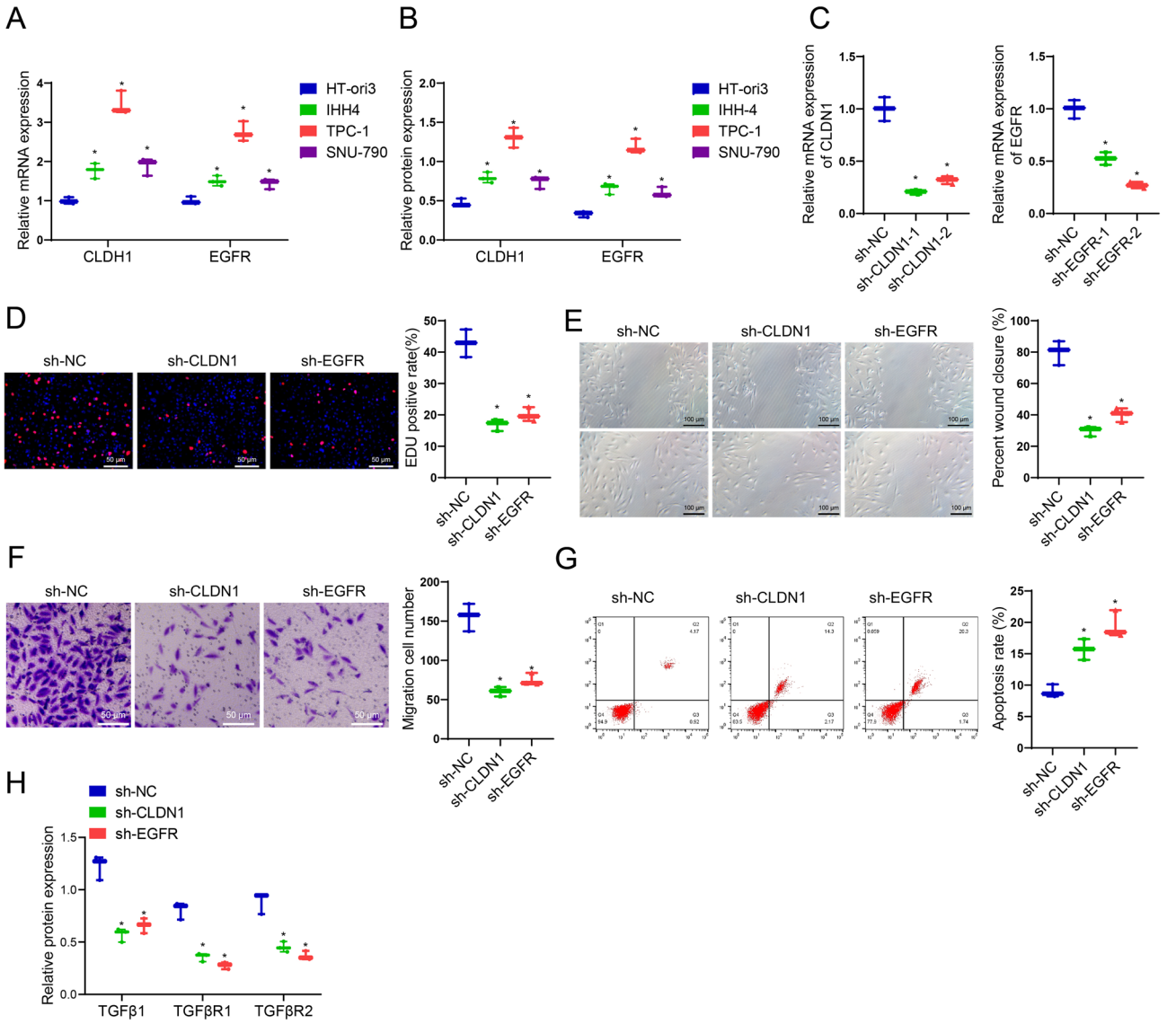

Fig. 5 The impact of CLDN1 and EGFR silencing on biological functions of TPC-1 cells. **A**, **B** qRT-PCR and WB were used to detect the levels of CLDN1 and EGFR mRNA and protein in normal thyroid epithelial cells (HT-ori3) and PTC cells (IHH-4, SNU-790, TPC-1); **C** qRT-PCR assessed the silencing efficiency of sh-CLDN1 and sh-EGFR; **D** EDU assay measured the proliferative capacity of PTC cells (scale bar = 50 μm); **E** scratch assay evaluated the migration ability of PTC cells (scale bar = 100 μm); **F** transwell assay assessed the invasive ability of PTC cells (scale bar = 50 μm); **G** flow cytometry determined the apoptotic rate of PTC cells; **H** WB analysis examined the expression of proteins related to the TGF-β receptor signaling pathway in the EMT process in different groups of PTC cells, including TGFβ1, TGFβR1, and TGFβR2. *Indicates $P < 0.05$ compared to the normal thyroid epithelial cells (HT-ori3) group or the sh-NC group, with experiments repeated three times

These results indicate that the silencing of CLDN1 and EGFR inhibits the tumor formation ability of thyroid papillary carcinoma cells and enhances $CD8^+$ T cell immune function.

This study provides an in-depth analysis of the expression and potential biological roles of CLDN1 and EGFR in PTC, enhancing our understanding of these molecules as key players in tumor progression and as potential therapeutic targets [15, 16]. Notably, our findings confirm the phenomenon of elevated expression of these molecules in PTC tissues compared to normal tissues, further illustrating their impact on tumor proliferation, invasion, and migration. Such insights underscore the clinical relevance of CLDN1 and EGFR, aligning with previous research to a degree yet presenting discrepancies possibly due to variations in sample sizes, geographical origins of samples, detection methods, or analytical techniques [42–44], thereby highlighting the complexity and challenges in correlating gene expression with clinical outcomes across diverse populations and study designs.

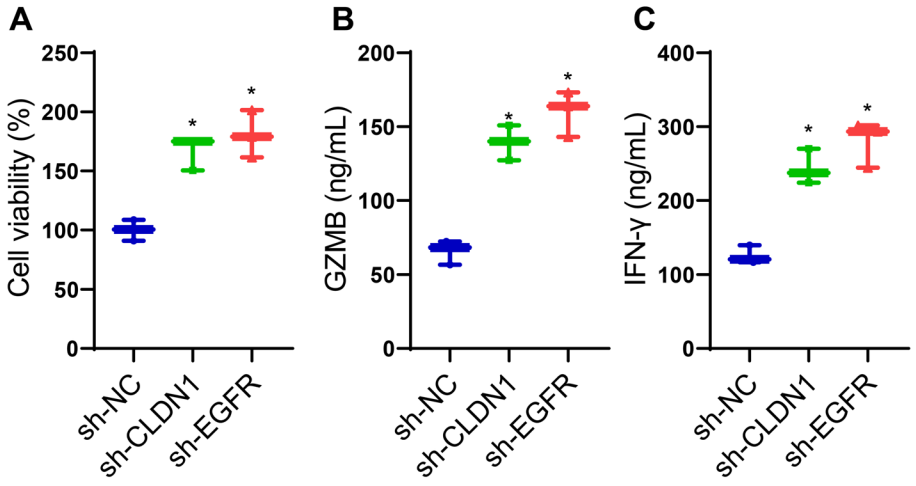

Fig. 6 Silencing of CLDN1 and EGFR in PTC cells enhances co-culture activity and cytotoxicity of $CD8^+$ T cells. **A** MTT assay measured the activity of co-cultured $CD8^+$ T cells; **B** ELISA assessed the level of GZMB in the cell culture medium; **C** ELISA determined the level of IFN-γ in the cell culture medium. *Indicates $P < 0.05$ compared to the sh-NC group, with experiments repeated three times

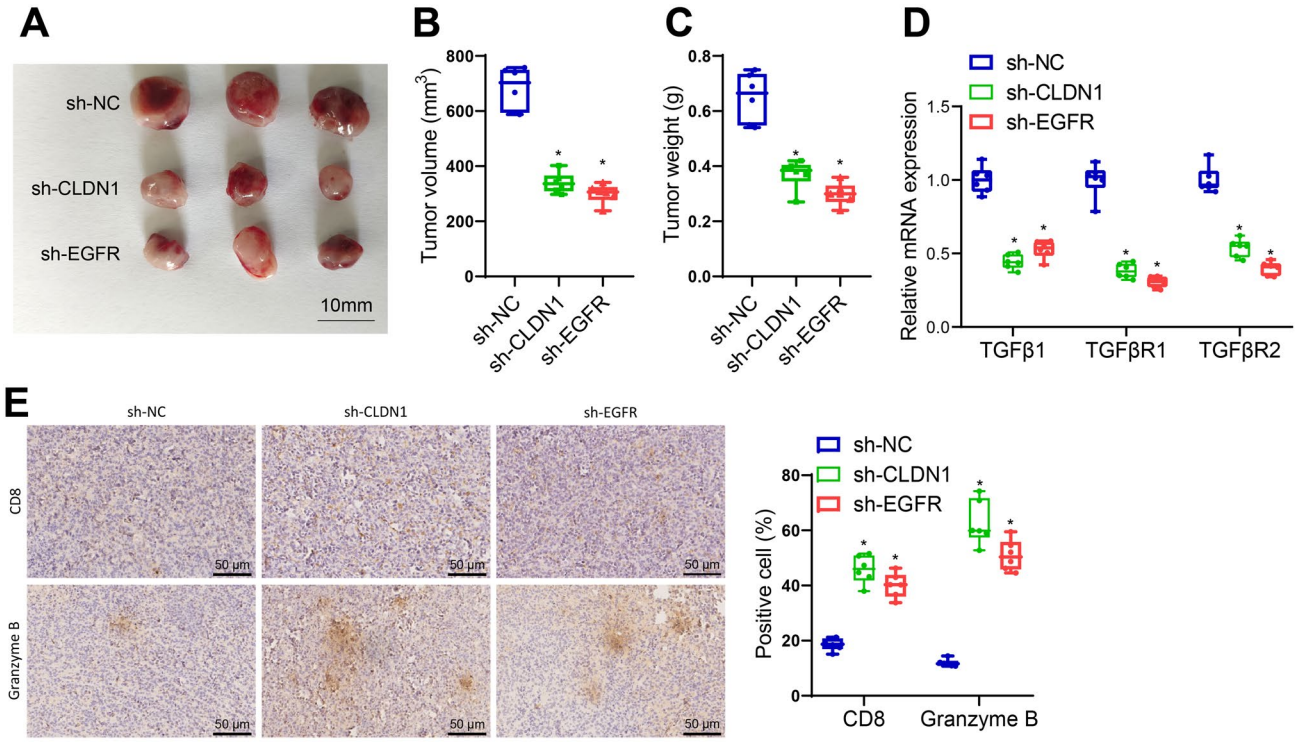

Fig. 7 The impact of CLDN1 and EGFR silencing on tumor formation ability of PTC cells and $CD8^+$ T cell immune function. **A** Morphology of mouse tumor tissues in each group; **B** volume of mouse tumor tissues in each group; **C** weight of mouse tumor tissues in each group; **D** WB analysis of the expression of proteins related to the TGF-β receptor signaling pathway in the EMT process in mouse tumor tissues, including TGFβ1, TGFβR1, and TGFβR2; **E** immunohistochemical staining to detect the expression of CD8 and granzyme B in mouse tumor tissue sections (scale bar 50 μm). *$P < 0.05$ compared to the sh-NC group. Each group consisted of 6 mice

Previous studies have suggested that CLDN1 induces EMT in nasopharyngeal carcinoma cells by upregulating β-catenin expression and promoting its nuclear localization [45]. Additionally, in pancreatic cancer, the EGFR/ERK/NF-κB signaling pathway mediates tumor EMT [46]. Our findings not only elucidate the expression patterns of CLDN1 and EGFR in PTC and their association with tumor development-related molecular pathways but also highlight their potentially significant roles in cancer progression, particularly in the EMT process. This provides novel insights and targets for future therapeutic strategies focusing on these pathways.

Moreover, our analysis indicates a significant association between high expression of CLDN1 and EGFR and adverse prognoses in PTC patients, suggesting a close link with clinical parameters such as tumor size, stage, and lymph node

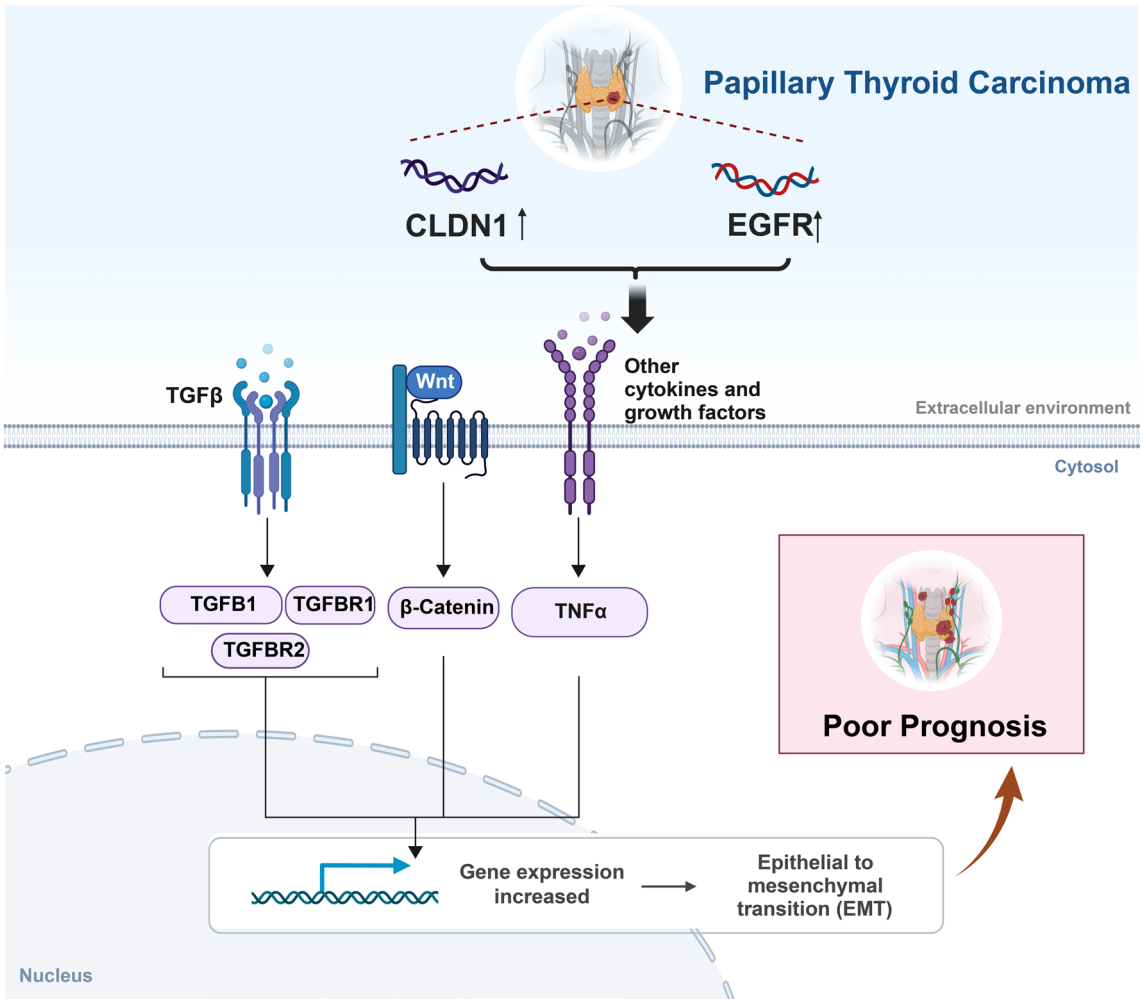

Fig. 8 Schematic diagram of CLDN1 and EGFR genes regulating EMT in PTC

metastasis. The observed reduction of $CD8^+$ T cells in the tumor microenvironment of high-expression cases suggests these genes may influence tumor immune evasion, potentially offering new avenues for immunotherapy strategies targeting tumor immune escape mechanisms [11, 47]. Additionally, the study establishes a significant correlation between CLDN1 and EGFR expression and the EMT process, implicating these genes in the regulation of PTC's invasiveness and metastatic capabilities.

Employing meta-analysis to integrate data from various studies has enhanced the reliability and generalizability of our results, revealing commonalities and differences across studies that contribute to a more comprehensive understanding of CLDN1 and EGFR's roles in PTC. However, it's crucial to acknowledge the limitations inherent to meta-analysis, such as data heterogeneity and potential publication bias, which must be considered when interpreting the findings.

This research innovatively analyzes CLDN1 and EGFR expression patterns, their association with clinical features, and their interactions with the tumor microenvironment and EMT process in PTC. This comprehensive analytical approach sheds new light on PTC's molecular mechanisms and presents significant molecular targets for the development of future clinical diagnostics and treatment strategies.

In summary, our findings corroborate the critical roles of CLDN1 and EGFR in PTC progression and substantiate their potential as biomarkers and therapeutic targets. While enriching our molecular understanding of PTC, these insights pave the way for new diagnostic and therapeutic directions. Nonetheless, this study's limitations, including restricted sample size and design constraints, may affect the interpretation and applicability of the results. Future research should address these limitations and further explore treatment strategies targeting CLDN1 and EGFR to improve clinical management and prognosis for PTC patients.

4 Conclusion

Based on the findings presented, we preliminarily conclude that CLDN1 and EGFR may serve as potential biomarkers and therapeutic targets for PTC. Furthermore, the expression of CLDN1 and EGFR is closely associated with immune cell infiltration, including $CD8^+$ T cells, and the EMT process in tumors (Fig. 8). This study, employing a combination of high-throughput transcriptomic sequencing, proteomic data, and meta-analysis, highlights the clinical relevance of CLDN1 and EGFR in PTC and lays a new theoretical foundation for their role as potential biomarkers and therapeutic targets. However, it is important to note that this study primarily relies on public databases for data collection, and despite analyzing a large dataset, it lacks validation through clinical trials. Future biological experiments and clinical studies are necessary to assess the clinical utility of CLDN1 and EGFR in PTC management further.

Acknowledgements None.

Author contributions JunJie Wu and YouMei Wang conceived and designed the study. Lei Yan performed the bioinformatics analyses and conducted the meta-analysis. YaWen Dong supervised the experiments, including cell culture, MTT assays, and immunohistochemistry. All authors contributed to the writing and revision of the manuscript and approved the final version for publication.

Funding This study was supported by Pinghu City Science and Technology Project (Ping Science and Technology [2022] No. 7 Social Development Category General-21).

Data availability The datasets generated and/or analyzed during the current study are available from the corresponding author on reasonable request.

Declarations

Ethics approval and consent to participate The animal experimental processes were approved by the Ethnic Committee of The First People's Hospital of Pinghu (2022-001) and conducted in strict accordance with the standard of the Guide for the Care and Use of Laboratory Animals published by the Ministry of Science and Technology of the People's Republic of China in 2006.

Consent for publication Not applicable.

Competing interests The authors declare no competing interests.

References

1. Houten PV, Netea-Maier RT, Smit JW. Differentiated thyroid carcinoma: an update. Best Pract Res Clin Endocrinol Metab. 2023;37(1):101687. https://doi.org/10.1016/j.beem.2022.101687.
2. Wei X, Wang X, Xiong J, et al. Risk and prognostic factors for $BRAF^{V600E}$ mutations in papillary thyroid carcinoma. Biomed Res Int. 2022;2022:9959649. https://doi.org/10.1155/2022/9959649.
3. Lam AK. Papillary thyroid carcinoma: current position in epidemiology, genomics, and classification. Methods Mol Biol. 2022;2534:1–15. https://doi.org/10.1007/978-1-0716-2505-7_1.
4. Hong S, Xie Y, Cheng Z, et al. Distinct molecular subtypes of papillary thyroid carcinoma and gene signature with diagnostic capability. Oncogene. 2022;41(47):5121–32. https://doi.org/10.1038/s41388-022-02499-0.
5. Volpi EM, Ramirez-Ortega MC, Carrillo JF. Editorial: Recent advances in papillary thyroid carcinoma: progression, treatment and survival predictors. Front Endocrinol. 2023;14:1163309. https://doi.org/10.3389/fendo.2023.1163309.
6. Herrera M, Hussein MH, Persons E, et al. Survival benefits of extensive surgery in patients with papillary thyroid microcarcinoma. Am J Surg. 2024;229:99–105. https://doi.org/10.1016/j.amjsurg.2023.11.001.
7. Liao M, Wang Z, Yao J, Xing H, Hao Y, Qiu B. Identification of potential biomarkers for papillary thyroid carcinoma by comprehensive bioinformatics analysis. Mol Cell Biochem. 2023;478(9):2111–23. https://doi.org/10.1007/s11010-022-04606-x.

8. Scheffel RS, Dora JM, Maia AL. BRAF mutations in thyroid cancer. Curr Opin Oncol. 2022;34(1):9–18. https://doi.org/10.1097/CCO.0000000000000797.
9. Pitsava G, Stratakis CA, Faucz FR. PRKAR1A and thyroid tumors. Cancers. 2021;13(15):3834. https://doi.org/10.3390/cancers13153834.
10. Póvoa AA, Teixeira E, Bella-Cueto MR, et al. Genetic determinants for prediction of outcome of patients with papillary thyroid carcinoma. Cancers. 2021;13(9):2048. https://doi.org/10.3390/cancers13092048.
11. Sagnak Yilmaz Z, Sarioglu S. Molecular pathology of micropapillary carcinomas: is characteristic morphology related to molecular mechanisms? Appl Immunohistochem Mol Morphol. 2023;31(5):267–77. https://doi.org/10.1097/PAI.0000000000001123.
12. Huang J, Zhang L, He C, et al. Claudin-1 enhances tumor proliferation and metastasis by regulating cell anoikis in gastric cancer. Oncotarget. 2015;6(3):1652–65. https://doi.org/10.18632/oncotarget.2936.
13. Piontek A, Eichner M, Zwanziger D, et al. Targeting claudin-overexpressing thyroid and lung cancer by modified *Clostridium perfringens* enterotoxin. Mol Oncol. 2020;14(2):261–76. https://doi.org/10.1002/1878-0261.12615.
14. Jorissen RN, Walker F, Pouliot N, Garrett TP, Ward CW, Burgess AW. Epidermal growth factor receptor: mechanisms of activation and signalling. Exp Cell Res. 2003;284(1):31–53. https://doi.org/10.1016/s0014-4827(02)00098-8.
15. So CW, Sourisseau M, Sarwar S, Evans MJ, Randall G. Roles of epidermal growth factor receptor, claudin-1 and occludin in multi-step entry of hepatitis C virus into polarized hepatoma spheroids. PLoS Pathog. 2023;19(12): e1011887. https://doi.org/10.1371/journal.ppat.1011887.
16. Jiang G, Fang H, Shang X, Chen X, Cao F. CHFR-mediated epithelial-to-mesenchymal transition promotes metastasis in human breast cancer cells. Mol Med Rep. 2021;23(6):451. https://doi.org/10.3892/mmr.2021.12090.
17. Wu Y, Jha R, Li A, et al. Probiotics (*Lactobacillus plantarum* HNU082) supplementation relieves ulcerative colitis by affecting intestinal barrier functions, immunity-related gene expression, gut microbiota, and metabolic pathways in mice. Microbiol Spectr. 2022;10(6): e0165122. https://doi.org/10.1128/spectrum.01651-22.
18. Fatima I, Uppada JP, Chhonker YS, et al. Identification and characterization of a first-generation inhibitor of claudin-1 in colon cancer progression and metastasis. Biomed Pharmacother. 2023;159: 114255. https://doi.org/10.1016/j.biopha.2023.114255.
19. Lopes-Gonçalves G, Costa-Pessoa JM, Pimenta R, et al. Evaluation of glomerular sirtuin-1 and claudin-1 in the pathophysiology of non-diabetic focal segmental glomerulosclerosis. Sci Rep. 2023;13(1):22685. https://doi.org/10.1038/s41598-023-49861-0.
20. Subramanian A, Tamayo P, Mootha VK, et al. Gene set enrichment analysis: a knowledge-based approach for interpreting genome-wide expression profiles. Proc Natl Acad Sci USA. 2005;102(43):15545–50. https://doi.org/10.1073/pnas.0506580102.
21. Cerami E, Gao J, Dogrusoz U, et al. The cBio cancer genomics portal: an open platform for exploring multidimensional cancer genomics data [published correction appears in Cancer Discov. 2012;2(10):960]. Cancer Discov. 2012;2(5):401–4. https://doi.org/10.1158/2159-8290.CD-12-0095.
22. Pontén F, Jirström K, Uhlen M. The human protein atlas—a tool for pathology. J Pathol. 2008;216(4):387–93. https://doi.org/10.1002/path.2440.
23. Ozdamar B, Bose R, Barrios-Rodiles M, Wang HR, Zhang Y, Wrana JL. Regulation of the polarity protein Par6 by TGFbeta receptors controls epithelial cell plasticity. Science. 2005;307(5715):1603–9. https://doi.org/10.1126/science.1105718.
24. Balduzzi S, Rücker G, Schwarzer G. How to perform a meta-analysis with R: a practical tutorial. Evid Based Ment Health. 2019;22(4):153–60. https://doi.org/10.1136/ebmental-2019-300117.
25. Yi S, Liu L, Chen Z. lncRNA EGFEM1P promotes thyroid cancer progression by acting as an miR-369-3p sponge and upregulating TCF4. Oncol Lett. 2022;24(6):456. https://doi.org/10.3892/ol.2022.13576.
26. Xie M, Yu T, Jing X, et al. Exosomal circSHKBP1 promotes gastric cancer progression via regulating the miR-582-3p/HUR/VEGF axis and suppressing HSP90 degradation. Mol Cancer. 2020;19(1):112. https://doi.org/10.1186/s12943-020-01208-3.
27. Wang JJ, Siu MK, Jiang YX, et al. Aberrant upregulation of PDK1 in ovarian cancer cells impairs $CD8^+$ T cell function and survival through elevation of PD-L1. Oncoimmunology. 2019;8(11): e1659092. https://doi.org/10.1080/2162402X.2019.1659092.
28. Zhang L, Xu B, Qiang Y, et al. Overexpression of deubiquitinating enzyme USP28 promoted non-small cell lung cancer growth. J Cell Mol Med. 2015;19(4):799–805. https://doi.org/10.1111/jcmm.12426.
29. Jiang D, Gong F, Ge X, et al. Neuron-derived exosomes-transmitted miR-124-3p protect traumatically injured spinal cord by suppressing the activation of neurotoxic microglia and astrocytes. J Nanobiotechnol. 2020;18(1):105. https://doi.org/10.1186/s12951-020-00665-8.
30. Li F, Song W, Wu L, Liu B, Du X. EIF4A3 induced circGRIK2 promotes the malignancy of glioma by regulating the miR-1303/HOXA10 axis. Am J Cancer Res. 2023;13(12):5868–86.
31. Feng G, Chen C, Luo Y. PRMT1 accelerates cell proliferation, migration, and tumor growth by upregulating ZEB1/H4R3me2as in thyroid carcinoma. Oncol Rep. 2023;50(6):210. https://doi.org/10.3892/or.2023.8647.
32. Zhang X, Zhang L, Wang B, et al. GLP-1 receptor agonist liraglutide inhibits the proliferation and migration of thyroid cancer cells. Cell Mol Biol. 2023;69(14):221–5. https://doi.org/10.14715/cmb/2023.69.14.37.
33. Wang Y, Yang H, Su X, et al. SREBP2 promotes the viability, proliferation, and migration and inhibits apoptosis in TGF-β1-induced airway smooth muscle cells by regulating TLR2/NF-κB/NFATc1/ABCA1 regulatory network. Bioengineered. 2022;13(2):3137–47. https://doi.org/10.1080/21655979.2022.2026550.
34. Zhao F, Qu Y, Zhu J, et al. miR-30d-5p plays an important role in autophagy and apoptosis in developing rat brains after hypoxic-ischemic injury. J Neuropathol Exp Neurol. 2017;76(8):709–19. https://doi.org/10.1093/jnen/nlx052.
35. Yamashita AS, Geraldo MV, Fuziwara CS, et al. Notch pathway is activated by MAPK signaling and influences papillary thyroid cancer proliferation. Transl Oncol. 2013;6(2):197–205. https://doi.org/10.1593/tlo.12442.
36. Wang F, Wu L, Yin L, Shi H, Gu Y, Xing N. Combined treatment with anti-PSMA CAR NK-92 cell and anti-PD-L1 monoclonal antibody enhances the antitumour efficacy against castration-resistant prostate cancer. Clin Transl Med. 2022;12(6): e901. https://doi.org/10.1002/ctm2.901.
37. Zeng Z, Tang S, Chen L, Hou H, Liu Y, Li J. LncRNA HAGLROS contribute to papillary thyroid cancer progression by modulating miR-206/HMGA2 expression. Aging. 2023;15(24):14930–44. https://doi.org/10.18632/aging.205321.
38. Li YJ, Chen X, Kwan TK, et al. Dietary fiber protects against diabetic nephropathy through short-chain fatty acid-mediated activation of G protein-coupled receptors GPR43 and GPR109A. J Am Soc Nephrol. 2020;31(6):1267–81. https://doi.org/10.1681/ASN.2019101029.

39. Kurz KS, Kalmbach S, Ott M, Staiger AM, Ott G, Horn H. Follicular lymphoma in the 5th edition of the WHO-classification of haematolymphoid neoplasms-updated classification and new biological data. Cancers. 2023;15(3):785. https://doi.org/10.3390/cancers15030785.
40. Vasko V, Espinosa AV, Scouten W, et al. Gene expression and functional evidence of epithelial-to-mesenchymal transition in papillary thyroid carcinoma invasion. Proc Natl Acad Sci USA. 2007;104(8):2803–8. https://doi.org/10.1073/pnas.0610733104.
41. McKenzie MD, Dudek NL, Mariana L, et al. Perforin and Fas induced by IFNgamma and TNFalpha mediate beta cell death by OT-I CTL. Int Immunol. 2006;18(6):837–46. https://doi.org/10.1093/intimm/dxl020.
42. Chen J, Spracklen CN, Marenne G, et al. The trans-ancestral genomic architecture of glycemic traits. Nat Genet. 2021;53(6):840–60. https://doi.org/10.1038/s41588-021-00852-9.
43. Giacomini E, Scotti GM, Vanni VS, et al. Global transcriptomic changes occur in uterine fluid-derived extracellular vesicles during the endometrial window for embryo implantation. Hum Reprod. 2021;36(8):2249–74. https://doi.org/10.1093/humrep/deab123.
44. Berg LM, Gurr C, Leyhausen J, et al. The neuroanatomical substrates of autism and ADHD and their link to putative genomic underpinnings. Mol Autism. 2023;14(1):36. https://doi.org/10.1186/s13229-023-00568-z.
45. Wu X, Xiao J, Zhao C, et al. Claudin1 promotes the proliferation, invasion and migration of nasopharyngeal carcinoma cells by upregulating the expression and nuclear entry of β-catenin. Exp Ther Med. 2018;16(4):3445–51. https://doi.org/10.3892/etm.2018.6619.
46. Wang L, Wang L, Zhang H, et al. AREG mediates the epithelial-mesenchymal transition in pancreatic cancer cells via the EGFR/ERK/NF-κB signalling pathway. Oncol Rep. 2020;43(5):1558–68. https://doi.org/10.3892/or.2020.7523.
47. Beekhof R, Bertotti A, Böttger F, et al. Phosphoproteomics of patient-derived xenografts identifies targets and markers associated with sensitivity and resistance to EGFR blockade in colorectal cancer. Sci Transl Med. 2023;15(709): eabm3687. https://doi.org/10.1126/scitranslmed.abm3687.